IOPscience iopscience.iop.org

Home Search Collections Journals About Contact us My IOPscience

Theory of Zener-photon resonances in the transport of two-band semiconductor superlattices

This article has been downloaded from IOPscience. Please scroll down to see the full text article.

2001 J. Phys.: Condens. Matter 13 3157

(http://iopscience.iop.org/0953-8984/13/13/324)

View the table of contents for this issue, or go to the journal homepage for more

Download details:
IP Address: 171.66.16.226
The article was downloaded on 16/05/2010 at 11:46

Please note that terms and conditions apply.

INSTITUTE OF PHYSICS PUBLISHING JOURNAL OF PHYSICS: CONDENSED MATTER

J. Phys.: Condens. Matter **13** (2001) 3157–3167 www.iop.org/Journals/cm PII: S0953-8984(01)20071-X

Theory of Zener-photon resonances in the transport of two-band semiconductor superlattices

P Kleinert[1] **and V V Bryksin**[2]

[1] Paul-Drude-Institut für Festkörperelektronik, Hausvogteiplatz 5–7, 10117 Berlin, Germany
[2] Physical Technical Institute, Politekhnicheskaya 26, 194021 St Petersburg, Russia

E-mail: kl@pdi-berlin.de

Received 14 December 2000, in final form 18 January 2001

Abstract

Using the density-matrix approach, we study intersubband tunnelling in superlattices subject to both dc and ac electric fields aligned perpendicular to the layers. Zener-photon resonances and dynamic localization are identified both in the carrier occupation numbers and the current density. While a global, time-averaged population inversion cannot occur in the simple two-band model considered, a temporal inversion is predicted to appear due to strong ac fields in the THz range. At the Zener-photon resonances, the THz field may generate appreciable gain.

1. Introduction

The dynamics of charged carriers in a superlattice (SL) under the action of both dc and ac electric fields has been the subject of intensive research. Electromagnetic radiation in the THz regime (0.1–10 THz) covers the important energy range of intersubband transitions in quantum-confined semiconductor heterostructures, which is extremely important for infrared emission and detector applications. Under definite conditions, the carriers are predicted to reveal a variety of time-dependent phenomena such as Bloch oscillations [1], intersubband Zener tunnelling [2, 3] and absolute negative conductance near zero bias [4, 5]. In particular, the phenomenon of dynamic localization has received a great deal of attention [6–8].

In the presence of a high dc electric field, an electron in a single miniband is predicted to execute Bloch oscillations. Without any collisions, they move along closed orbits and no longer contribute to the stationary carrier transport, which leads to negative differential conductivity. In this transport regime, carrier scattering, which enables transport, plays an important role. If an additional ac field in the THz range is applied to the SL, resonant delocalization of carriers occurs for a Bloch frequency $\Omega_{dc} = eE_{dc}d/\hbar$ (E_{dc} is the strength of the dc field and d the SL period) equal to an integer multiple of the THz frequency ω. This may result in considerable gain and cause photon-assisted dc transport. However, the related current–voltage (I–V) characteristics and the shape of the resonance peaks are singular in character as long as lifetime broadening is not taken into account. Most of the theoretical

0953-8984/01/133157+11$30.00 © 2001 IOP Publishing Ltd Printed in the UK

studies treated collisional broadening in the constant relaxation-time approximation and relied on the Tien–Gordon or Tucker formula [9, 10] in their calculation of the transport properties under THz irradiation [11–15]. All these theoretical treatments are essentially one dimensional in nature and do not recognize the fact that carrier scattering by impurities, by phonons and among themselves makes the problem truly three dimensional. This may lead to results that are significantly different from those of one-dimensional models. Within a balance-equation approach, impurity and phonon scattering have been treated adequately in [16]. However, the balance equations are not designed to cope with the Wannier–Stark (WS) localization, which becomes essential at high electric field strengths. Quantum effects, such as cyclotron-Stark-phonon–photon resonances, which are described beyond the semiclassical transport model, have been studied recently within the density-matrix approach [17, 18]. Using the semiconductor Bloch equations, fractional WS ladders have been predicted to occur, when the ratio of the Bloch frequency Ω_{dc} to the ac-field frequency ω becomes a fractional number [19].

Additional interesting resonance phenomena are expected to appear in the SL transport, when the interminiband dynamics is considered. Coherent effects have been treated, which are induced by alternating electric fields. One interesting phenomenon is the collapse of quasi-energy bands [6–8], which is nothing but a signature of dynamical localization. Coherent transport has been studied within a one-dimensional model [3]. At avoided crossings of the two interpenetrating WS ladders, coherent oscillations between the minibands occur, which are called tunnelling or intersubband Zener resonances. The destruction of Zener resonances and Bloch oscillations in random external fields has been studied within the density-matrix approach [20]. The assumption of no dissipation made by the afore-mentioned authors seems to be inadequate for interpreting experimental results in real systems. Rather, it is expected that scattering processes play a crucial role in almost all current contributions arising in a multisubband system. This will be demonstrated in the present paper, in which we identify various tunnelling- and scattering-induced current contributions related to the external dc and ac fields. While tunnelling is treated in a rigorous quantum-mechanical manner, we will consider scattering within the simple relaxation-time approximation. That means, we follow former theoretical studies by neglecting the heating of the lateral electron motion. This simple one-dimensional model has not been chosen to give an accurate representation of real systems. It is our intent here to use a model simple enough for a clear identification of current contributions originating from tunnelling or scattering events. When the subbands are decoupled from each other, our approach reproduces the widely used quasiclassical description [11–15] of intraminiband transport in SLs subject to dc and ac electric fields.

2. Solution of the kinetic equation and calculation of the carrier density

The time-averaged current density for carrier motion along the SL axis is calculated from the Wigner-transformed, intraband distribution function $f_\nu^\nu(\vec{k}, t)$ (with ν being the subband index). The explicit spatial dependence describing field-domain formation is not taken into account. In the expression for the current density

$$j_z = \frac{en}{\hbar} \sum_{\vec{k}\nu} \frac{\partial \varepsilon_\nu(\vec{k})}{\partial k_z} \frac{\omega}{2\pi} \int_0^{2\pi/\omega} \mathrm{d}t \; f_\nu^\nu(\vec{k}, t) \tag{1}$$

besides the time-averaged distribution function, the gradient of the dispersion relation $\varepsilon_\nu(\vec{k})$ of the νth miniband appears. We consider a simple two-band tight-binding SL model

$$\varepsilon_1(\vec{k}) = \frac{\hbar^2 \vec{k}_\perp^2}{2m} + \frac{\Delta_1}{2}(1 - \cos k_z d) \tag{2}$$

$$\varepsilon_2(\vec{k}) = \frac{\hbar^2\vec{k}_\perp^2}{2m} + \varepsilon_g + \frac{\Delta_2}{2}(1+\cos k_z d) \tag{3}$$

with Δ_1 (Δ_2) being the width of the lower (upper) miniband and ε_g the mini-gap energy. For simplicity, we do not consider a possible nonparabolicity of the lateral electron motion, which we will characterize by only one effective mass m. In equation (1), n denotes the total electron density, while in equations (2) and (3) $\vec{k}_\perp$ represents the wave-vector within the SL layers. The kinetic equation for the Wigner-transformed elements of the density matrix $f_\nu^{\nu'}(\vec{k},t)$ is given by [21]

$$\left\{\frac{\partial}{\partial t} + \frac{\mathrm{i}}{\hbar}[\varepsilon_{\nu'}(\vec{k}) - \varepsilon_\nu(\vec{k})] + \frac{e}{\hbar}\vec{E}(t)\nabla_{\vec{k}}\right\} f_\nu^{\nu'}(\vec{k},t)$$
$$+\frac{\mathrm{i}e\vec{E}(t)}{\hbar}\sum_\mu[\vec{Q}_{\mu\nu}(\vec{k})f_\mu^{\nu'}(\vec{k},t) - \vec{Q}_{\nu'\mu}(\vec{k})f_\nu^\mu(\vec{k},t)]$$
$$= \sum_{\mu\mu'}\sum_{\vec{k}_1} f_\mu^{\mu'}(\vec{k}_1,t)W_{\mu\nu}^{\mu'\nu'}(\vec{k}_1,\vec{k}\mid t) \tag{4}$$

where the dipole matrix elements

$$\vec{Q}_{\mu\mu'}(\vec{k}) = -\mathrm{i}\sum_{\vec{K}}\chi_{\mu'}(\vec{k}+\vec{K})\nabla_k\chi_\mu^*(\vec{k}+\vec{K}) \tag{5}$$

determine the wavefunction overlap calculated from the SL envelope functions χ_μ. The Q-term in equation (4) is related to the confining SL potential via the wavefunction χ_μ. Coupling constants of scattering processes do not enter this contribution, which describes tunnelling under the mutual influence of dc and ac electric fields

$$E(t) = E_{dc} + E_{ac}\cos(\omega t) \tag{6}$$

the strengths of which can be expressed by the Bloch frequencies Ω_{dc} and $\Omega_{ac} = eE_{ac}d/\hbar$. Besides intersubband tunnelling, there are scattering-induced intra- and intersubband electron transitions characterized by the scattering probabilities $W_{\mu'\nu'}^{\mu\nu}$. Quite similar to the tunnelling contribution in equation (4), we have scattering-induced terms, which are associated with the off-diagonal elements of the density matrix $f_\nu^{\nu'}$ (with $\nu' \neq \nu$). The related scattering probabilities have the form $W_{\mu\mu}^{\nu\nu}$ and are treated within the simple constant relaxation-time approximation

$$W_{\nu\nu}^{\mu\mu}(\vec{k}',\vec{k}) \to -\frac{\delta_{\vec{k},\vec{k}'}}{\tau}. \tag{7}$$

Intersubband transitions due to carrier generation and recombination are treated in a similar way by

$$W_{12}^{12}(\vec{k}',\vec{k}) \to \frac{\delta_{\vec{k},\vec{k}'}}{\tau_{12}} \qquad W_{21}^{21}(\vec{k}',\vec{k}) \to \frac{\delta_{\vec{k},\vec{k}'}}{\tau_{21}} \tag{8}$$

where the scattering times τ_{12} and τ_{21} are related to each other by the equation $\tau_{12} = \tau_{21} \times \exp(\varepsilon_g/k_BT)$.

The set of kinetic equations for the elements of the density matrix simplifies considerably in the relaxation-time approximation and takes the form

$$\left(\frac{\partial}{\partial t} + \frac{e\vec{E}(t)}{\hbar}\nabla_{\vec{k}}\right) f_\nu^\nu(\vec{k},t) \pm \mathrm{i}\frac{e\vec{E}(t)}{\hbar}[\vec{Q}_{21}f_2^1(\vec{k},t) - \vec{Q}_{12}f_1^2(\vec{k},t)]$$
$$= -\frac{1}{\tau_\nu}(f_\nu^\nu(\vec{k},t) - f_\nu^{(0)}(\vec{k})) \mp \frac{1}{\tau_{12}}f_1^1(\vec{k},t) \pm \frac{1}{\tau_{21}}f_2^2(\vec{k},t) \tag{9}$$

$$\left(\frac{\partial}{\partial t} + \frac{\mathrm{i}}{\hbar}(\varepsilon_1(\vec{k}) - \varepsilon_2(\vec{k})) + \frac{1}{\tau} + \frac{e\vec{E}(t)}{\hbar}\nabla_{\vec{k}}\right) f_2^1(\vec{k},t) = \mathrm{i}\frac{e\vec{E}(t)}{\hbar}\vec{Q}_{12}[f_2^2(\vec{k},t) - f_1^1(\vec{k},t)] \tag{10}$$

with τ_ν being the intrasubband scattering time and $f_\nu^{(0)}$ an appropriate mean distribution function, which is associated with the scattering-out term. In equation (9), the upper (lower) sign refers to $\nu = 1$ ($\nu = 2$). Recently, a similar model has been studied by Zhao *et al* [22, 23], who identified the well known intrasubband current contribution and treated tunnelling effects numerically. In contrast to their numerical study, we are able to carry out calculations analytically to a late stage, permitting a clear identification of various tunnelling- and scattering-induced current contributions. In addition, based on our density-matrix description, we are in the position to derive analytic results valid in some interesting limiting cases. Unfortunately, Zhao *et al* [22, 23] did not discriminate between intra- and intersubband scattering times. Taking into account that intra- and intersubband dissipation mechanisms differ from each other remarkably, the validity of this approximation has to be strongly questioned. Intrasubband scattering times are usually much smaller than intersubband relaxation times [24, 25]. In our study, we focus on GaAs–AlGaAs SLs composed of narrow quantum wells, where the subband separation energy is larger than the longitudinal–optical (LO) phonon energy. There is general agreement that the intersubband relaxation of such systems is dominated by LO phonon scattering and that the intersubband relaxation time is of the order of picoseconds [24–28]. In our numerical analysis, we will rely on scattering-time parameters that are in the range of the most typical parameters used in estimations for quantum-cascade lasers [29–33]. Whereas scattering is treated in the relatively crude relaxation-time approximation, the electric-field induced tunnelling is adequately described by the set of kinetic equations (9) and (10). To reproduce well known results derived within the Esaki–Tsu model [34], we will follow the reasoning in the literature [11, 12] by identifying $f_\nu^{(0)}$ as the equilibrium distribution function.

To solve equations (9) and (10), we exploit the symmetry properties of the distribution function [17] ($f_\nu^{\nu'}(k_z + 2\pi/d, t) = f_\nu^{\nu'}(k_z, t)$ and $f_\nu^{\nu'}(k_z, t + 2\pi/\omega) = f_\nu^{\nu'}(k_z, t)$) by making use of the Fourier transformation

$$f_\nu^{\nu'}(\vec{k}, t) = \sum_{l,m=-\infty}^{\infty} \mathrm{e}^{\mathrm{i}lk_z d}\, \mathrm{e}^{\mathrm{i}m\omega t} f_\nu^{\nu'}(l, m). \tag{11}$$

For constant dipole matrix elements, we obtain the following coupled set of equations for the diagonal elements of the density matrix:

$$\begin{aligned}
&\mathrm{i}(m\omega + l\Omega_{dc}) f_\nu^\nu(l, m) + \frac{\mathrm{i}}{2} l\Omega_{ac}(f_\nu^\nu(l, m+1) + f_\nu^\nu(l, m-1)) \\
&\qquad \pm \mathrm{i}\frac{eE_{dc}}{\hbar}[Q_{21} f_2^1(l, m) - Q_{12} f_1^2(l, m)] \\
&\qquad \pm \frac{\mathrm{i}}{2}\frac{eE_{ac}}{\hbar}[Q_{21}(f_2^1(l, m-1) + f_2^1(l, m+1)) - Q_{12}(f_1^2(l, m-1) + f_1^2(l, m+1))] \\
&\qquad = -\frac{1}{\tau_\nu}(f_\nu^\nu(l, m) - \delta_{m,0} f_\nu^{(0)}(l)) \mp \frac{1}{\tau_{12}} f_1^1(l, m) \pm \frac{1}{\tau_{21}} f_2^2(l, m)
\end{aligned} \tag{12}$$

which will be solved numerically to determine the time-dependent mean occupation numbers $f_\nu^\nu(l = 0, m)$ ($m = 0, \pm 1, \pm 2, \ldots$). The Fourier components of the equilibrium distribution function are given by

$$f_\nu^{(0)}(l) = \pm \frac{I_l(\Delta_\nu/(2k_B T))}{I_0(\Delta_\nu/(2k_B T))} F_\nu \tag{13}$$

where $F_\nu = f_\nu^\nu(l = 0, m = 0)$ denotes the occupation probability of the subband ν and I_l are modified Bessel functions. The off-diagonal elements of the density matrix enter the kinetic equation (12). These elements will be determined analytically under the condition of strong dc electric fields ($\Omega_{dc}\tau_{eff} \gg 1$, where τ_{eff} is an effective scattering time).

We obtain (see the appendix)

$$f_2^1(l,m) = \frac{e}{\hbar}\vec{E}_{dc}\vec{Q}_{12}\sum_{l',m'=-\infty}^{\infty}\sum_{k=-\infty}^{\infty}(-1)^{m-m'}J_{m-m'}\left(l'\frac{\Omega_{ac}}{\omega}\right)J_{m'-k}\left(l'\frac{\Omega_{ac}}{\omega}\right)$$
$$\times\frac{(-1)^{l'}J_{l-l'}((\Delta_1+\Delta_2)/2\hbar\Omega)J_{l'}((\Delta_1+\Delta_2)/2\hbar\Omega)}{m'\omega+l'\Omega_{dc}-\omega_{21}-\mathrm{i}/\tau}[f_2^2(0,k)-f_1^1(0,k)] \quad (14)$$

where the effective energy gap $\hbar\omega_{21}$ is calculated from

$$\hbar\omega_{21} = \varepsilon_g + \frac{\Delta_1+\Delta_2}{2}. \quad (15)$$

The complementary matrix element f_1^2 satisfies the symmetry relation

$$f_1^2(l,m) = f_2^1(-l,-m)^*. \quad (16)$$

From equations (12) and (14), several special cases can be derived. First, let us treat the carrier redistribution under the influence of a dc electric field ($\Omega_{ac} = 0$). In this case, we obtain immediately the solution

$$F_1 + F_2 = 1 \qquad F_2 = \frac{2\Omega_{dc}^2\tau A + 1/\tau_{12}}{4\Omega_{dc}^2\tau A + 1/\tau_{12} + 1/\tau_{21}} \quad (17)$$

in which the field dependent term A defined by

$$A = \left(\frac{Q_{12}}{d}\right)^2\sum_{l=-\infty}^{\infty}\frac{J_l((\Delta_1+\Delta_2)/2\hbar\Omega_{dc})^2}{(l\Omega_{dc}\tau-\omega_{21}\tau)^2+1} \quad (18)$$

may describe a considerable carrier redistribution at the intersubband tunnelling resonance $\Omega_{dc} = \omega_{21}$. However, as can be seen from equation (17), population inversion cannot occur in the simple two-band model. In order to account for the additional effect of an alternating field on the carrier redistribution, one has to go back to equations (12) and (14). Numerical results are presented and discussed in the next section.

To proceed further in the calculation of the current density, we apply the Fourier transformation of equation (11) to equation (1) and consider equations (2) and (3). We obtain

$$j_z = \frac{en_s}{2\hbar}\mathrm{Im}\,[\Delta_1 f_1^1(-1,0) - \Delta_2 f_2^2(-1,0)] \quad (19)$$

where n_s denotes the carrier sheet density. The density-matrix elements $f_\nu^\nu(-1,0)$ are calculated by transforming equation (12) back to the time domain. The resulting first-order differential equation for $f_\nu^\nu(l,t)$ is solved by taking into account periodic boundary conditions. Repeating the calculation outlined in the appendix of [17], we obtain in the limit $\tau_1 \approx \tau_2 \ll \tau_{12}, \tau_{21}$ the analytical result

$$f_\nu^\nu(l,m) = \sum_{k,m'=-\infty}^{\infty}\frac{J_{k-m}(l\Omega_{ac}/\omega)J_{k-m'}(l\Omega_{ac}/\omega)}{\mathrm{i}(l\Omega_{dc}+k\omega)+1/\tau_1}\Phi_\nu(l,m') \quad (20)$$

$$\Phi_\nu(l,m) = \frac{1}{\tau_1}\delta_{m,0}f_\nu^{(0)}(l) \mp \mathrm{i}\frac{eE_{dc}}{\hbar}[Q_{21}f_2^1(l,m) - Q_{12}f_1^2(l,m)]$$
$$\mp\frac{\mathrm{i}}{2}\frac{eE_{ac}}{\hbar}[Q_{21}(f_2^1(l,m-1)+f_2^1(l,m+1)) - Q_{12}(f_1^2(l,m-1)+f_1^2(l,m+1))] \quad (21)$$

in which off-diagonal elements of the density matrix appear. Inserting equation (20) together with (21) into equation (19), various current contributions can be identified.

The first term on the right-hand side of equation (21) gives rise to the following scattering-induced current contribution of the νth subband:

$$j_{z,\nu}^{(s)} = \frac{en_s\Delta_\nu}{2\hbar}\frac{I_1(\Delta_\nu/(2k_BT))}{I_0(\Delta_\nu/(2k_BT))}F_\nu\sum_{k=-\infty}^{\infty}J_k\left(\frac{\Omega_{ac}}{\omega}\right)^2\frac{(\Omega_{dc}+k\omega)\tau_1}{((\Omega_{dc}+k\omega)\tau_1)^2+1} \tag{22}$$

which can be expressed in the widely used Tien–Gordon [9] or Tucker [10] form as

$$j_{z\nu}^{(s)}(\Omega_{dc},\Omega_{ac}) = \sum_{k=-\infty}^{\infty}J_k\left(\frac{\Omega_{ac}}{\omega}\right)^2 j_{z\nu}^{ET}(\Omega_{dc}+k\omega) \tag{23}$$

with $j_{z\nu}^{ET}$ being the dc current density of the Esaki–Tsu model [34] applied to one subband.

The second term on the right-hand side of equation (21) is associated with tunnelling induced by the dc electric field and modified by the THz field. In the absence of the ac field ($\Omega_{ac}=0$), one obtains for the tunnelling current

$$j_z^{(t)} = \frac{2en_s}{\tau}(F_1-F_2)\left(\frac{Q_{12}}{d}\right)^2\sum_{l=-\infty}^{\infty}lJ_l\left(\frac{\Delta_1+\Delta_2}{2\hbar\Omega_{dc}}\right)^2\frac{(\Omega_{dc}\tau)^2}{(l\Omega_{dc}\tau-\omega_{21}\tau)^2+1} \tag{24}$$

which may exhibit sharp peaks at the tunnelling resonances $l\Omega_{dc}=\omega_{21}$ ($l=1,2,\ldots$).

The last contribution appearing in Φ_ν, which is proportional to E_{ac}, gives rise to tunnelling events induced by the ac field. The related current density plays only a minor role in our present approach, in which we focus on the case $\Omega_{ac}\ll\Omega_{dc}$.

3. Numerical results and discussion

We will start our numerical analysis of tunnelling in SLs under the influence of both dc and ac electric fields by treating the field-dependent redistribution of carriers between the two subbands. Solving the set of linear equations (12) and (14), we will focus on the global occupation numbers $F_\nu(t)=f_\nu^\nu(l=0,t)$. Figure 1 shows the time-averaged occupation numbers of the lower (F_1) and upper (F_2) subband as a function of the dc electric field. In the absence of the THz field (dashed line), a sizable redistribution is observed at the tunnelling resonance $\Omega_{dc}=\omega_{21}$ marked by a vertical line. At this field strength, the upper and lower subbands are almost equally populated. However, it is seen from equation (17) that population inversion cannot occur. The application of an additional ac field in the THz regime leads to photon sidebands or combined Zener-photon resonances at $\Omega_{dc}\pm m\omega=\omega_{21}$, which are marked by vertical dashed lines. The thick solid line has been calculated with an Ω_{ac} value that fulfills the equation $J_0(\Omega_{ac}/\omega)=0$. In this case, the dynamical localization leads to a complete disappearance of the main resonance at $\Omega_{dc}=\omega_{21}$. This applies also to the nth photon replica, when $J_n(\Omega_{ac}/\omega)=0$ is satisfied. This is illustrated by the thin solid line, where we have $J_1(\Omega_{ac}/\omega)=0$ so that the photon replica at $\Omega_{dc}\pm\omega=\omega_{21}$ disappears.

The time-dependent occupation number of the upper subband is shown in figure 2, where the field strength E_{ac} was incremented in 15 steps from 1 to 4 kV cm^{-1} as indicated. F_ν as a function of ωt is periodic with the period 2π. The dc electric field strength satisfies the tunnelling resonance condition $\Omega_{dc}=\omega_{21}$. The subband occupation almost equilibrates in the considered case. It is expected and confirmed by our numerical calculation that a THz field cannot give rise to a time-averaged global population inversion. However, as shown in figure 2, a global population inversion may temporally occur due to the presence of the ac electric field. The appearance of this interesting effect depends sensitively on the scattering times used in the calculation. With decreasing intrasubband scattering time, the temporal inversion disappears. Therefore, more sophisticated calculations are necessary for a reliable prediction of such an effect.

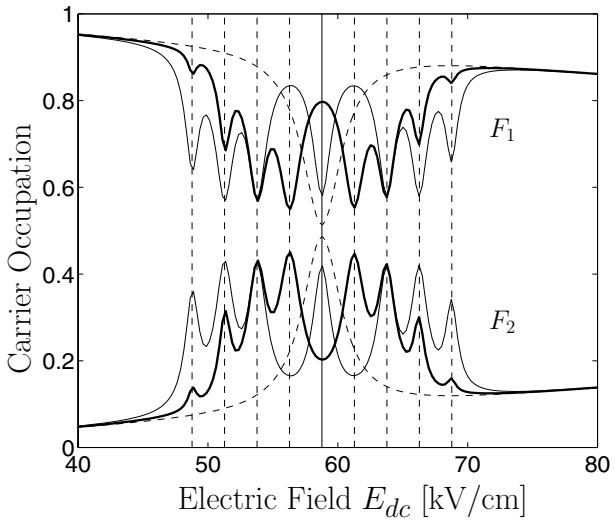

Figure 1. Occupation numbers of the lower (F_1) and upper (F_2) miniband as a function of the dc electric field. In the calculation, the following parameters have been used: $\varepsilon_g = 100$ meV, $\Delta_1 = 5$ meV, $\Delta_2 = 30$ meV, $\tau = 1$ ps, $\tau_{21} = 2$ ps, $\tau_1 = \tau_2 = 0.05$ ps, $\hbar\omega = 5$ meV and $T = 77$ K. The dashed line has been calculated with $E_{ac} = 0$. The thick and thin solid lines refer to the case of dynamic localization characterized by $J_0(\Omega_{ac}/\omega) = 0$ ($E_{ac} = 6.012$ kV cm^{-1}, $d = 20$ nm) and $J_1(\Omega_{ac}/\omega) = 0$ ($E_{ac} = 9.5793$ kV cm^{-1}, $d = 20$ nm), respectively. Vertical dashed lines mark the positions of Zener-photon resonances.

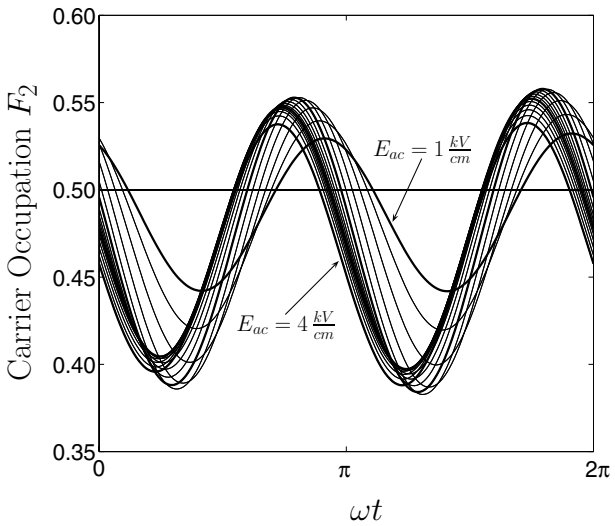

Figure 2. The occupation number of the upper miniband as a function of ωt for E_{ac} values ranging from 1 to 4 kV cm^{-1} incremented in 15 steps. The curves referring to $E_{ac} = 1, 2, 3$ and 4 kV cm^{-1} are plotted by thick lines. The set of parameters used in the calculation is given by: $\varepsilon_g = 100$ meV, $\Delta_1 = 5$ meV, $\Delta_2 = 50$ meV, $\tau = 2$ ps, $\tau_{21} = 1$ ps, $\tau_1 = \tau_2 = 1$ ps, $\hbar\omega = 2$ meV and $T = 77$ K. The dc electric field satisfies the tunnelling resonance condition $\Omega_{dc} = \omega_{21}$ ($E_{dc} = 63.7802$ kV cm^{-1}).

Numerical results for the current density calculated from equations (14), (19), and (20) are shown in figure 3 by the solid line. The main resonances appear at $l\Omega_{dc} = \omega_{21}$ ($l = 1, 2$).

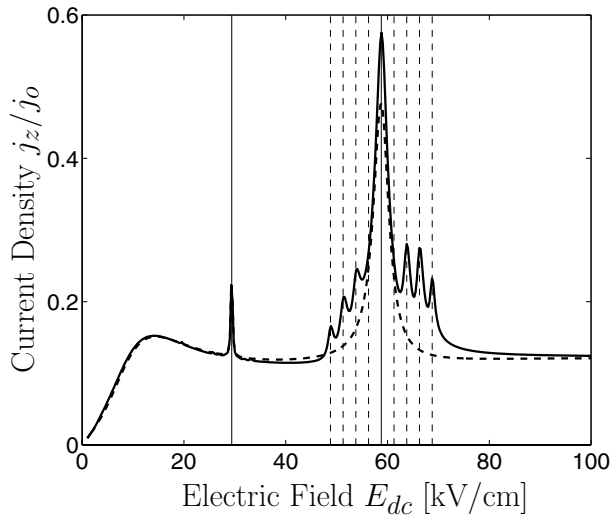

Figure 3. Relative current density j_z/j_0 (with $j_0 = 2en_s/\tau$) as a function of the dc electric field strength for $\varepsilon_g = 100$ meV, $\Delta_1 = 5$ meV, $\Delta_2 = 30$ meV, $\tau = 1$ ps, $\tau_{21} = 2$ ps, $\tau_1 = \tau_2 = 0.05$ ps, $\hbar\omega = 5$ meV and $T = 77$ K. The strength of the THz field satisfies the condition of dynamic localization $J_1(\Omega_{ac}/\omega) = 0$ ($E_{ac} = 9.5793$ kV cm^{-1}, $d = 20$ nm). The dashed line has been calculated from equation (22). Tunnelling and Zener-photon resonances are marked by vertical solid and dashed lines, respectively.

At the same time, the scattering-induced current contribution calculated from equation (22) exhibits sharp peaks (dashed line) due to the field dependence of the occupation numbers F_ν. For the chosen parameter set, photon replicas (marked by vertical dashed lines) group around the main tunnelling resonance. Again, we considered the case $J_1(\Omega_{ac}/\omega) = 0$, in which due to dynamic localization the replicas at $\Omega_{dc} \pm \omega = \omega_{21}$ do not appear. The analytic expression (14) for the off-diagonal elements of the density matrix has been derived under the assumption of high dc electric fields ($\Omega_{dc}\tau_{eff} \gg 1$). These quantities describe tunnelling events. As field-mediated tunnelling becomes ineffective at low dc electric fields, we think that our results are relevant at low field strengths, too.

Another example is shown in figure 4, where the current density is depicted as a function of the dc electric field strength. Here we used an intraband scattering time, which is ten times larger than the value used in the calculation for figure 3. The current density shown by the solid line exhibits sharp maxima at tunnelling and Zener-photon resonances marked by vertical solid and dashed lines, respectively. Due to dynamic localization, the resonances at $\Omega_{dc} \pm \omega = \omega_{21}$ (indicated by arrows) do not occur ($J_1(\Omega_{ac}/\omega) = 0$). For the parameters used in the calculation, the current density becomes negative near zero dc biases and pronounced Stark-photon resonances appear at $\Omega_{dc} = k\omega$. If the ac field is switched off (dashed line), both the peculiarities at zero bias and the combined Zener-photon resonances disappear completely. To be noted further is that the Esaki–Tsu peak at about 600 V cm^{-1} is much more pronounced than in figure 3. Especially in the region of the photon replicas, considerable gain is predicted to occur.

The Stark-photon resonances at $\Omega_{dc} = m\omega$ have been experimentally observed [4, 5, 35–37] and thoroughly studied on the basis of the Tucker formula given in equation (23). To the best of our knowledge, the observation of the predicted combined Zener-photon resonances, which appear beyond the Tucker approach and group around the tunnelling

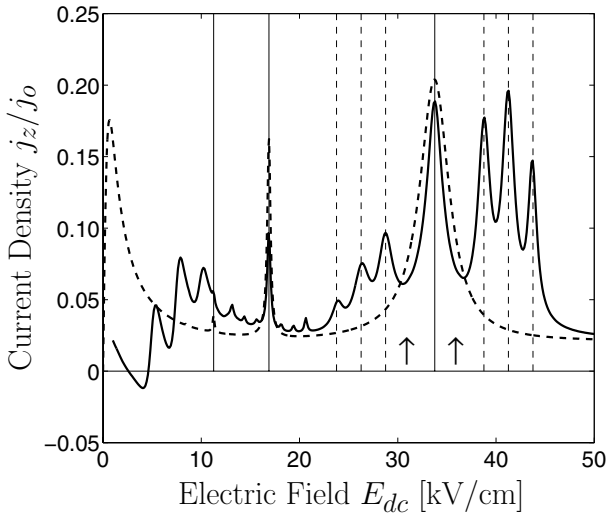

Figure 4. Relative current density as a function of the dc electric field strength for the same parameters as in figure 3 except for $\varepsilon_g = 50$ meV and $\tau_1 = \tau_2 = 0.5$ ps. The dashed line has been calculated with $E_{ac} = 0$. The arrows mark the positions of photon replicas at $\Omega_{dc} \pm \omega = \omega_{21}$, which are suppressed due to dynamic localization.

resonance, has not been reported up to now. Their identification may be masked by field-domain formation.

4. Summary

Within a simple two-band tight-binding model, we have studied the carrier redistribution and the electric current of a semiconductor SL subject to both dc and ac electric fields. Quantum mechanical tunnelling and scattering processes have been treated within the density-matrix approach. We focused our consideration on strong dc electric fields ($\Omega_{dc}\tau_{eff} \gg 1$) and relied on the relaxation-time approximation. Various scattering-induced current contributions as well as dc- and ac-field-mediated transport mechanisms due to tunnelling can be identified. The main tunnelling-related effect of an ac field in the THz range consists in the appearance of combined Zener-photon resonances at $\Omega_{dc} \pm m\omega = \omega_{21}$, which group around the tunnelling resonance. These resonances, which appear both in the field-induced carrier redistribution and the current density, may lead to considerable gain. At particular values of the parameter Ω_{ac}/ω ($J_m(\Omega_{ac}/\omega) = 0$), the effect of dynamical localization emerges. This leads to the disappearance of the mth photon replica in the field dependence of both the occupation number and the current density.

In the simple two-band model considered, a global population inversion cannot occur. However, we predict the appearance of a temporal global population inversion induced by the THz field and in the vicinity of the tunnelling resonance $\Omega_{dc} = \omega_{21}$. This dynamic effect depends sensitively on the value of the intrasubband scattering times. More refined model calculations are therefore necessary to confirm this prediction. A realistic microscopic treatment of scattering would also allow the consideration of other interesting phenomena such as the appearance of current anomalies due to phonon replicas [38].

Unfortunately, the experimental verification of our predictions may be hindered by field-domain formation in transport measurements. Another way to observe the predicted effects could be by using ultracold atoms in accelerating optical potentials.

Acknowledgments

The authors would like to acknowledge partial financial support by the Deutsches Zentrum für Luft- und Raumfahrt.

Appendix

In this appendix, we derive an analytical solution of equation (10) under the condition of strongly biased SLs. Introducing a new function $G(\vec{k},t)$ by

$$G(\vec{k},t) = f_2^1(\vec{k}_t,t) \qquad \vec{k}_t = \vec{k} + \int_0^t \mathrm{d}\tau\ \vec{E}_{ac}(\tau) \tag{A.1}$$

we obtain from equation (10)

$$\left(\frac{\partial}{\partial t} + \frac{\mathrm{i}}{\hbar}(\varepsilon_1(\vec{k}_t) - \varepsilon_2(\vec{k}_t)) + \frac{1}{\tau} + \frac{e\vec{E}_{dc}}{\hbar}\nabla_{\vec{k}}\right) G(\vec{k},t) = \mathrm{i}\frac{e\vec{E}(t)}{\hbar} Q_{12}[f_2^2(\vec{k}_t,t) - f_1^1(\vec{k}_t,t)] \tag{A.2}$$

in which only the constant electric field $\vec{E}_{dc}$ appears explicitly. In a second step, we introduce the function

$$f(\vec{k},t) = G(\vec{k},t)\exp\left(-\frac{\mathrm{i}}{eE_{dc}}\int_0^{k_{zt}} \mathrm{d}k_z'\,[\varepsilon_2(\vec{k}_\perp,k_z') - \varepsilon_1(\vec{k}_\perp,k_z') - \varepsilon_{21}(\vec{k}_\perp)]\right) \tag{A.3}$$

with

$$\varepsilon_{21}(\vec{k}_\perp) = \frac{d}{2\pi}\int_0^{2\pi/d} \mathrm{d}k_z\,(\varepsilon_2(\vec{k}) - \varepsilon_1(\vec{k})) \tag{A.4}$$

which fulfills a simple equation in Fourier space, when $\Omega_{ac}/\Omega_{dc} \ll 1$ is satisfied. By making use of the Fourier transformation

$$f(\vec{k},t) = \sum_{l=-\infty}^{\infty} \mathrm{e}^{\mathrm{i}lk_z d} f(\vec{k}_\perp,l,t) \tag{A.5}$$

we obtain in the limit $\Omega_{ac}/\Omega_{dc} \ll 1$

$$\left[\frac{\partial}{\partial t} + \mathrm{i}l\Omega_{dc} - \mathrm{i}\omega_{21} + \frac{1}{\tau}\right] f(\vec{k}_\perp,l,t) = \mathrm{i}Q_{12}\frac{eE(t)}{\hbar} \times \exp\left(\mathrm{i}l\frac{\Omega_{ac}}{\omega}\sin\omega t\right)\sum_{l_1=-\infty}^{\infty} J_{l_1-l}\left(\frac{\Delta_1+\Delta_2}{2\hbar\Omega_{dc}}\right)[f_2^2(\vec{k}_\perp,l_1,t) - f_1^1(\vec{k}_\perp,l_1,t)]. \tag{A.6}$$

Considering the equation

$$\exp\left(\mathrm{i}l\frac{\Omega_{ac}}{\omega}\sin\omega t\right) = \sum_{k=-\infty}^{\infty} J_k\left(l\frac{\Omega_{ac}}{\omega}\right)\mathrm{e}^{\mathrm{i}k\omega t} \tag{A.7}$$

we may easily Fourier transform equation (A.6) with respect to its time dependence. Under the condition of strong dc electric fields ($\Omega_{dc}\tau_{eff} \gg 1$), the $l = 0$ component of the distribution function dominates [21] ($f_v^v(l \neq 0, m) \ll f_v^v(l = 0, m)$) so that we obtain

$$f_{lm} = \Omega_{dc}\frac{Q_{12}}{d}\frac{J_{-l}((\Delta_1+\Delta_2)/2\hbar\Omega_{dc})}{m\omega + l\Omega_{dc} - \omega_{21} - \mathrm{i}/\tau}\sum_{k=-\infty}^{\infty} J_k\left(l\frac{\Omega_{ac}}{\omega}\right)[f_2^2(0,m-k) - f_1^1(0,m-k)]. \tag{A.8}$$

A Fourier transformation of equations (A.1) and (A.3) leads to

$$f_2^1(l,m) = \sum_{l_1,m_1=-\infty}^{\infty} (-1)^{m-m_1} J_{m-m_1}\left(l_1 \frac{\Omega_{ac}}{\omega}\right) J_{l-l_1}\left(\frac{\Delta_1+\Delta_2}{2\hbar\Omega_{dc}}\right) f_{l_1 m_1} \qquad \text{(A.9)}$$

in which we insert equation (A.8) to get our final result expressed by equation (14).

References

[1] Waschke C, Roskos H G, Schwedler R, Leo K, Kurz H and Köhler K 1993 *Phys. Rev. Lett.* **70** 3319
[2] Rotvig J, Jauho A P and Smith H 1995 *Phys. Rev. Lett.* **74** 1831
[3] Rotvig J, Jauho A P and Smith H 1996 *Phys. Rev.* B **54** 17 691
[4] Keay B J, Zeuner S, Allen S J, Maranowski K D, Gossard A C, Bhattacharya U and Rodwell M J W 1995 *Phys. Rev. Lett.* **75** 4102
[5] Keay B J, Allen S J, Galan J, Kaminski J P, Campman K L, Gossard A C, Bhattacharya U and Rodwell M J W 1995 *Phys. Rev. Lett.* **75** 4098
[6] Dunlap D H and Kenkre V M 1986 *Phys. Rev.* B **34** 3625
[7] Holthaus M and Hone D 1993 *Phys. Rev.* B **47** 6499
[8] Zhao X G 1996 *Commun. Theor. Phys.* **25** 233
[9] Tien P K and Gordon J P 1963 *Phys. Rev.* B **129** 647
[10] Tucker J R 1979 *IEEE J. Quantum Electron.* **15** 1234
[11] Ignatov A A, Schomburg E, Grenzer J, Renk K F and Dodin E P 1995 *Z. Phys.* B **98** 187
[12] Yevtushenko O M 1996 *Phys. Rev.* B **54** 2578
[13] Platero G and Aguado R 1997 *Appl. Phys. Lett.* **70** 3546
[14] Zhao X G, Georgaki G A and Niu Q 1997 *Phys. Rev.* B **56** 3976
[15] Wacker A, Jauho A P, Zeuner S and Allen S J 1997 *Phys. Rev.* B **56** 13 268
[16] Lei X S and Cui H L 1998 *Eur. Phys. J.* B **4** 513
[17] Bryksin V V and Kleinert P 1999 *Phys. Rev.* B **59** 8152
[18] Kleinert P and Bryksin V V 1999 *J. Phys.: Condens. Matter* **11** 2539
[19] Yan W X, Zhao X G and Wang H 1998 *J. Phys.: Condens. Matter* **10** L11
[20] Suqing D and Zhao X G 1999 *J. Phys.: Condens. Matter* **11** 7259
[21] Bryksin V V, Woloschin V C and Rajtzev A W 1980 *Fiz. Tverd. Tela* **22** 3076 (Engl. transl. *Sov. Phys.–Solid State* **22** 1796)
[22] Zhao X G and Hone D W 2000 *Phys. Rev.* B **62** 5010
[23] Suqing D, Zhang W and Zhao X G 2000 *Phys. Rev.* B **62** 9943
[24] Kisin M V, Gorfinkel V B, Stroscio M A, Belenky G and Luryi S 1997 *J. Appl. Phys.* **82** 2031
[25] Friedman L and Soref R A 1998 *J. Appl. Phys.* **83** 3480
[26] Tatham M C, Ryan J F and Foxon C T 1989 *Phys. Rev. Lett.* **63** 1637
[27] Morris D, Houde D, Deveand B and Regreny A 1994 *Superlatt. Microstruct.* **15** 309
[28] Levenson J A, Dolique G, Oudar J L and Abram I 1990 *Phys. Rev.* B **41** 3688
[29] Faist J, Capasso F, Sivco D L, Hutchinson L, Sirtori C, Chu S N G and Cho A Y 1994 *Appl. Phys. Lett.* **65** 2901
[30] Faist J, Capasso F, Sirtori C, Sivco D L, Hutchinson L and Cho A Y 1995 *Appl. Phys. Lett.* **66** 538
[31] Faist J, Capasso F, Sirtori C, Sivco D L, Baillargeon J N, Hutchinson L, Chu S N G and Cho A Y 1996 *Appl. Phys. Lett.* **68** 3680
[32] Sirtori C, Faist J, Capasso F, Sivco D L, Hutchinson A L and Cho A Y 1996 *Appl. Phys. Lett.* **69** 2810
[33] Slivken S, Litvinov V I, Razeghi M and Meyer J R 1999 *J. Appl. Phys.* **85** 665
[34] Suris R A and Shchamkhalova B S 1984 *Fiz. Tekh. Poluprovodn.* **18** 1178 (Engl. transl. *Sov. Phys.–Semicond.* **18** 738)
[35] Zeuner S, Keay B J, Allen S J, Maranowski K D, Gossard A C, Bhattacharya U and Rodwell M J W 1996 *Phys. Rev.* B **53** R1717
[36] Unterrainer K, Keay B J, Wanke M C, Allen S J, Leonard D, Medeiros-Ribeiro G, Bhattacharya U and Rodwell M J W 1996 *Phys. Rev. Lett.* **76** 2973
[37] Zeuner S, Keay B J, Allen S J, Maranowski K D, Gossard A C, Bhattacharya U and Rodwell M J W 1997 *Superlatt. Microstruct.* **22** 149
[38] Kleinert P 2000 *J. Phys.: Condens. Matter* **12** 8467